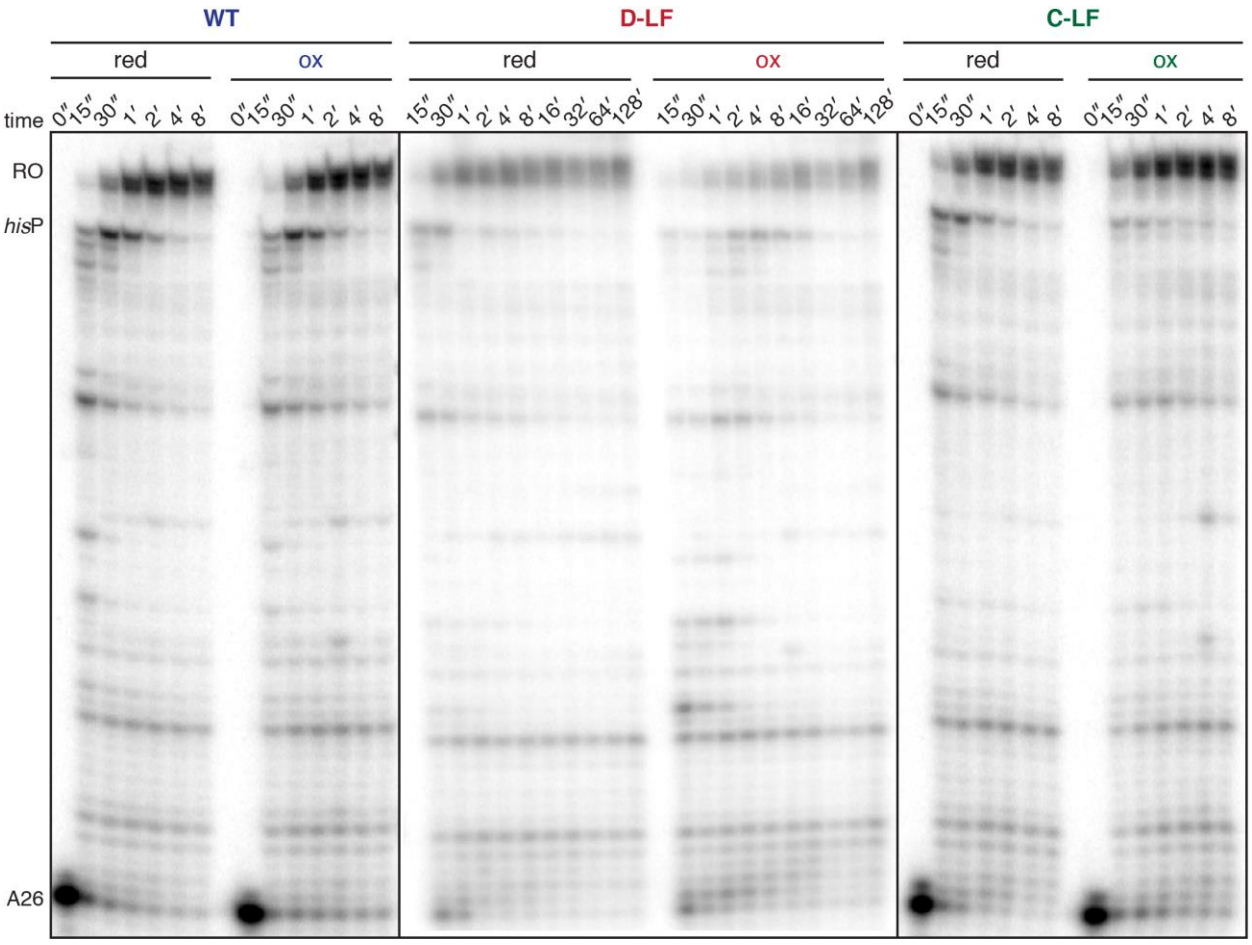

Figure S1. Constraining the clamp perturbs overall elongation rates through effects on relative pause strength. Representative gels showing the transcriptional behavior of WT, D-LF, and C-LF ECs under reducing and oxidizing conditions. RO, template run-off.

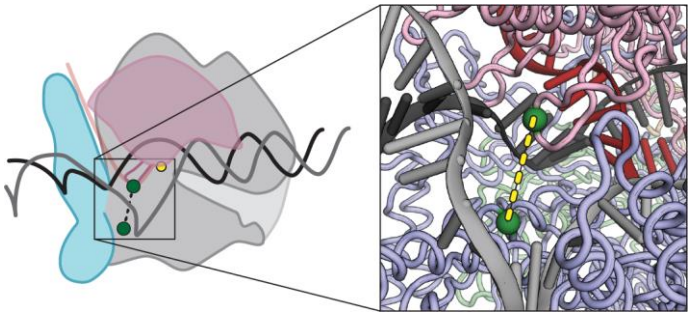

Figure S2. T-RP forms a disulfide crosslink within the transcription bubble. Left panel; position of the cysteine substitutions within the context of the entire EC. Right panel: zoomed-in view of the rudder-protrusion crosslink. Cα atoms are depicted as green spheres. A full nucleic-acid scaffold is modeled in based upon previous structural predictions [65] (RNA, red; template DNA, black; nontemplate, gray).

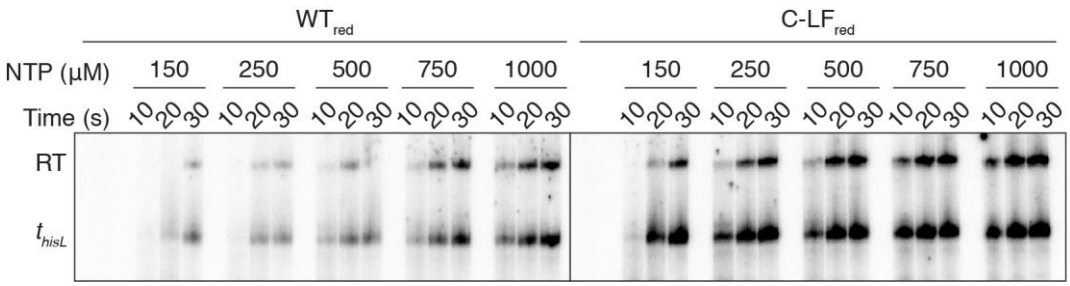

Figure S3. Elongation to t_{hisL} from A26 with different NTP concentrations under reducing conditions.

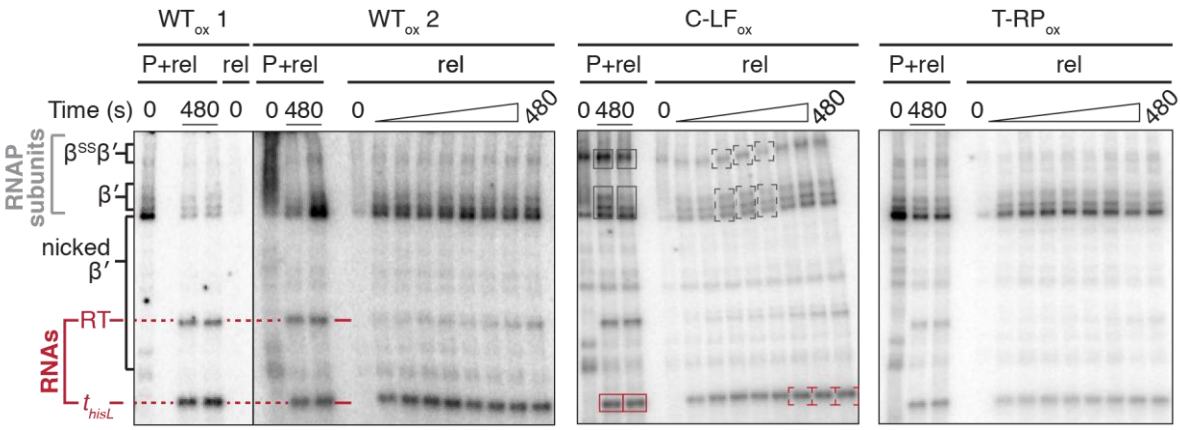

Figure S4. Representative dissociation assay non-reducing gels. P, bead-bound pellet; rel, sample released into the reaction supernatant. Two sets of P+rel (total sample) and 0 s timepoints of rel samples for WT ECs are shown on the left ($WT_{ox}1$ and $WT_{ox}2$) with replicate P+rel samples from the 480 s timepoint in adjacent lanes. As seen in $WT_{ox}2$, aggregation sometimes complicated measurements of total sample RNAP amounts. RNAs used for quantitation are marked in red: t_{hisL}, terminated RNA; RT, readthough RNA formed when ECs reach the end of the template. Proteolytic nicking of β′ generated minor and variable amounts of C-terminal ^{32}P-labeled bands (nicked β′); these bands were not used for quantitiation. Because quantitation relied on comparison of the amounts of β′ or RNA in the total vs. supernatant fractions, the small amount of nicked β′ did not interfere with quantitation. Multiple full-length β′ bands sometimes appeared because the gels were not run under reducing conditions to allow detection of the crosslinked β′. We included these variant β′ bands, which likely reflect internal disulfide formation, when quantifying released RNAP. Release timepoints taken at 0, 20, 30, 40, 50, 60, 120, 240, and 480 s. The C-LF gel (middle panel) is marked with examples of the bands used to quantify RNA and RNAP release efficiencies. Red boxes and brackets indicate RNA species at t_{hisL}; dark gray boxes and brackets indicate the ^{32}P-β′ and ^{32}P-β^{SS}β′ bands. For this example, RNA release efficiency was calculated as the ^{32}P signal minus background in red brackets divided by

the average ^{32}P signal minus background in the two red boxes. RNAP release efficiency is calculated as the ^{32}P signal minus background in dark gray brackets divided by the ^{32}P signal minus background in the dark gray boxes, multiplied by the termination efficiency to account for ECs that read through the terminator signal and did not release from the beads.

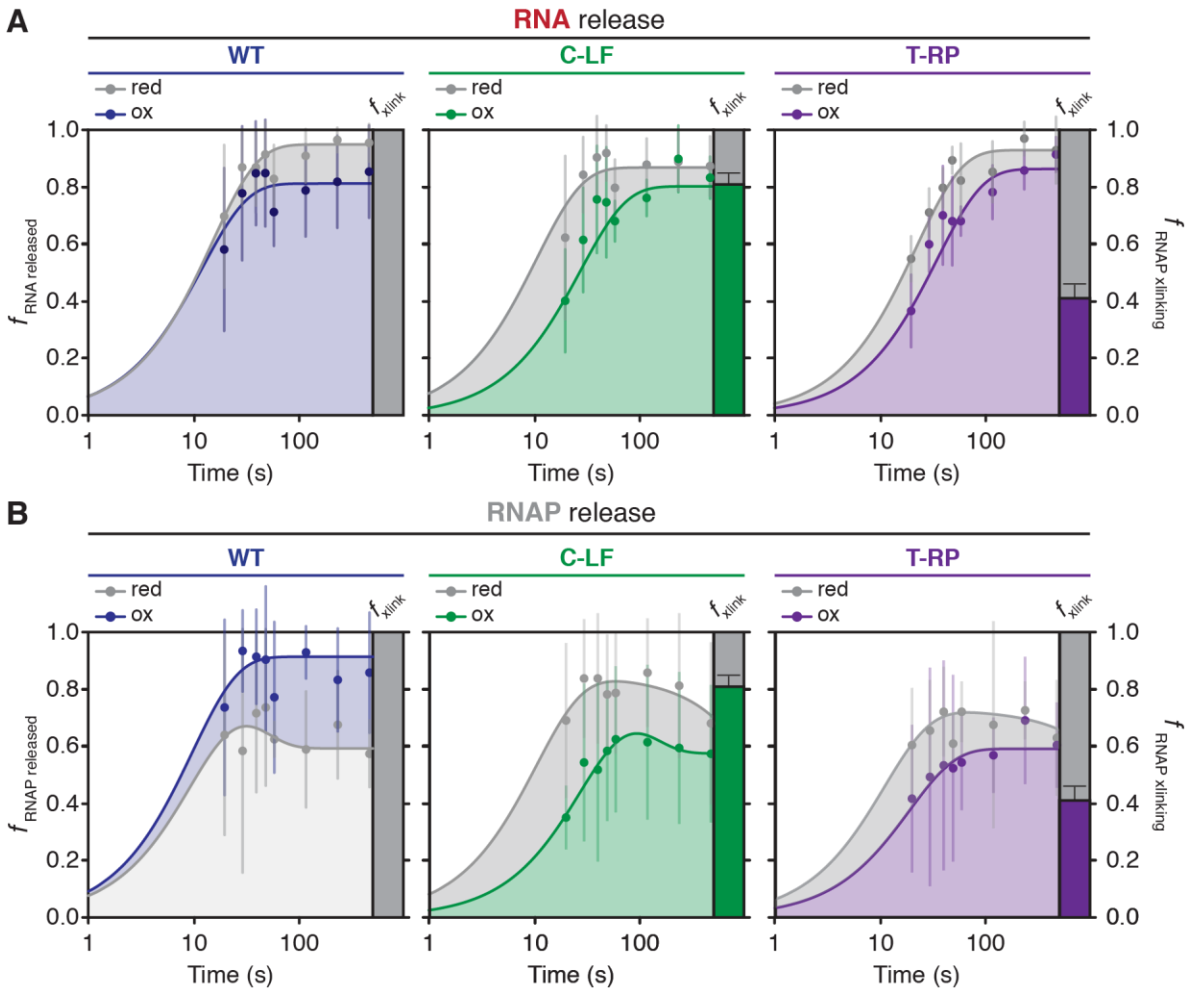

Figure S5. Evaluation of RNA and RNAP dissociation rates. (**A**) Semi-log plots of RNA release rates at t_{hisL}. RNA dissociation was determined as the fraction of RNA released into the reaction supernatant relative to total RNA at the terminator site. Data were fit to either a single exponential [$y = A(1 - e^{-kt})$] function. The y-axis label "efficiency" represents measurements of both Cys-pair crosslinking efficiency and RNA release efficiency. Bars to the right of plots represent crosslinking efficiencies under oxidizing conditions. Grey curves represent fits for RNA release under reducing conditions; colored curves represent fits under oxidizing conditions. Error bars represent the standard deviation at n = 3. (**B**) Semi-log plots of RNAP release at t_{hisL}. RNAP dissociation was determined as the fraction of RNAP released into the reaction supernatant relative to total RNAP within the reaction mixture multiplied by the TE. Data were

fit to the double exponential function $y = A_1(1 - e^{-k_1 t}) + A_2(1 - e^{-k_2 t})$. Plot components are the same as in subpanel A.

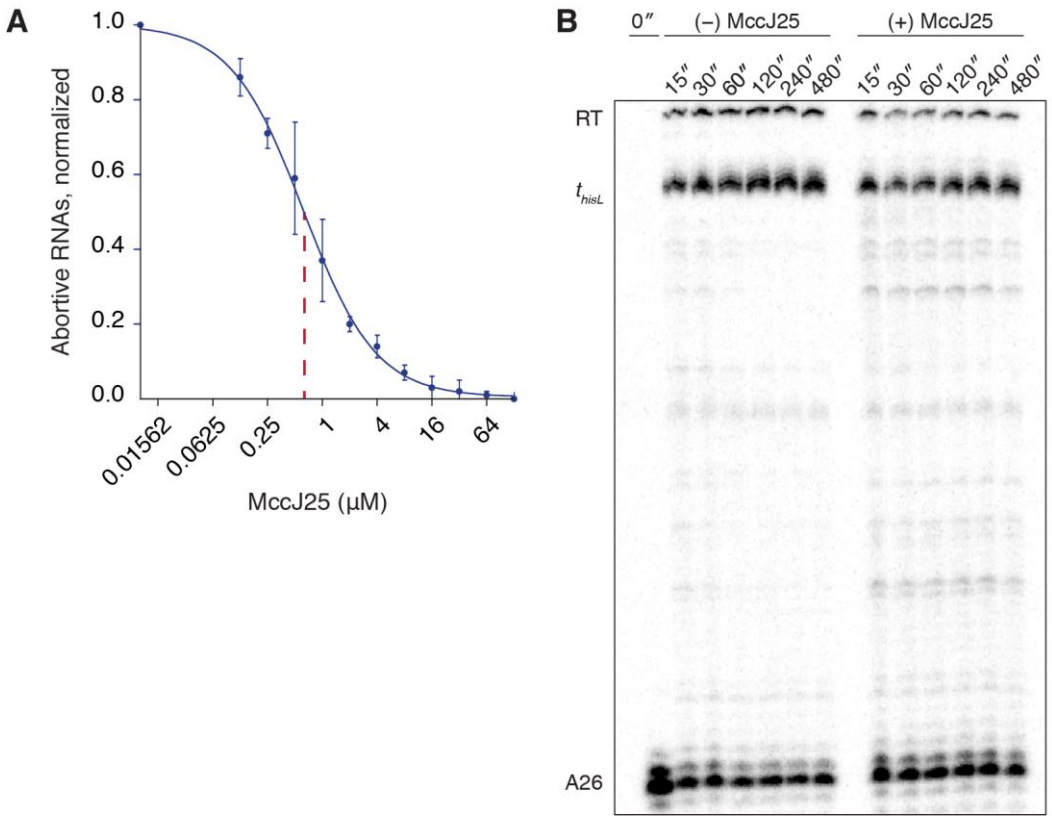

Figure S6. Effects of MccJ25 on RNAP during abortive initiation and elongation. (**A**) Abortive initiation by WT RNAP at *lac*UV5 is inhibited by MccJ25. Abortive products were normalized to the maximum signal in the absence of MccJ25. (**B**) Representative gel showing that the addition of MccJ25 to *in vitro* transcription assays at 5 s is sufficient time to allow elongation by the majority of ECs to t_{hisL} under conditions of saturating NTP concentration. The presence and persistence of pause bands in the +MccJ25 samples indicates successful arrest of lagging ECs by the inhibitor.

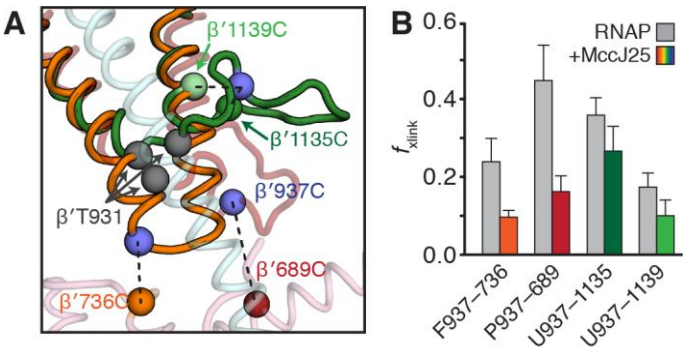

Figure S7. Cysteine-pair reporting suggests MccJ25 binds the TL in its unfolded conformation. (**A**) Location of TL cysteine-pairs. Three TL conformations observed in crystal structures were aligned to a cryo-EM structure of the *E. coli* EC [27]: orange, folded trigger helices, PDB ID: **2O5J** [8]; red, partially-folded TL, PDB ID: **2NVQ** [66]; green, unfolded TL, PDB ID: **1IW7** [38]. The bridge helix is depicted in cyan. Spheres depict the Cα atoms of relevant β′ residues. Grey spheres indicate the position of β′T931, a residue that when mutated (T931I) confers full resistance to MccJ25 and is thus likely a critical MccJ25 binding determinant. (**B**) Crosslinking efficiencies of cysteine-pair reporters in the absence (grey bars) and presence (colored bars) of MccJ25. Error represents the standard deviation (n=3).